Biosensors and Bioelectronics ■ (■■■■) ■■■–■■■

Contents lists available at ScienceDirect

Biosensors and Bioelectronics

journal homepage: www.elsevier.com/locate/bios

New ZnO nanostructures as non-enzymatic glucose biosensors

Aliakbar Tarlani [a,*], Mahtab Fallah [a], Behzad Lotfi [a], Avideh Khazraei [a], Sommayeh Golsanamlou [a], Jacques Muzart [b], Maryam Mirza-Aghayan [a]

[a] Chemistry & Chemical Engineering Research Center of Iran (CCERCI), Pazhouhesh Blvd., 17th Km. of Tehran- Karaj Highway, Tehran, Iran
[b] Institut de Chimie Moléculaire de Reims, CNRS-Université de Reims Champagne-Ardenne, BP 1039 51687, Reims cedex 2, France

ARTICLE INFO

Article history:
Received 14 June 2014
Received in revised form
7 September 2014
Accepted 22 September 2014

Keywords:
Zinc oxide
Solvothermal
Amino acid
Glucose
Nanobiosensor
Non-enzymatic

ABSTRACT

In a new approach, shape controlled synthesis of zinc oxide nanostructures were carried out using a solvothermal route assisted amino acids such as L-Lysine (lysine), L-Cysteine (cysteine) and L-Arginine (arginine) as bifunctional species with (or without) urea or oxalic acid as additives which affect the pH of the reaction. Rod, powder, particle, cube, rock candy-like, sheet, sphere, brain-like, groundnut-like and pussy willow-like morphologies were obtained through the synthetic route. Particle sizes varied from 25 nm to 4 μm. To test the application, nine ZnO nanostructures, formulated by multi-walled carbon nanotube (MWCNT) on glassy carbon electrode (GCE) were applied as new nanobiosensors for detecting glucose in a simple and inexpensive way without using any glucose oxidase or nafion. Glucose sensing accomplished in a phosphate buffer solution (PBS, pH=7) for ZnO/MWCNT/GCE samples. Results showed that in this non-enzymatic biosensor system, spherical ZnO obtained from zinc acetate/cycteine/oxalic acid synthetic route has the highest sensitivity of 64.29 μA/cm^2 mM with repeatable results. For the mentioned sensor, no interference observed in the presence of dopamine, uric acid and fructose.

1. Introduction

In the past decade, immense effort has been done for the synthesis of metal oxide nanostructures. Among the metal oxides, zinc oxide has attracted the attention of many scientists for mainly two reasons, Firstly, zinc oxide has unique piezoelectric (Li et al., 2012; Wang, 2007), pyroelectric (Wang, 2008) and semiconducting (Pan and Feng, 2008) properties, and secondly, has a large family of nanostructures allowing the synthesis of derivatives presenting various morphologies. Varied zero dimensional (Liu and Tong, 2008), one dimensional (Shen et al., 2007), two dimensional (Deng et al., 2005) and three dimensional (Shi et al., 2009) nanostructures of zinc oxide such as quantum dots (Lu et al., 2006), nanorods (Liu and Zeng, 2003), nanorings (Kong et al., 2004), nanohelices (Kong and Wang, 2003), nanoribbons (Botello-Méndez et al., 2008), nanowires (Morales and Lieber, 1998; Ng et al., 2003; Pan et al., 2004; Wang et al., 2005), nanopropellers (Gao and Wang, 2004), nanonails (Lao et al., 2003), nanoshells (De La Rica and Matsui, 2008) and other fascinating structures (Kong et al., 2004) have been reported so far. These nanostructures have different applications in biomedical sciences (Kim et al., 2010) as well as biosensors (Cui et al., 2001), solar cells (Briseno et al., 2010; Lee et al., 2008), nanotransistors (Ju et al., 2007), nanoresonators (Kumar et al., 2011) and photocatalyst (Akhavan, 2010; Nam et al., 2010).

Nanostructures of zinc oxide have been synthesized in both solvent and gas phases. However, methods in gas phase (Dai et al., 2003) are more complicated and expensive than those insolvent phase. Through the different methods, thermal evaporation (Tandra et al., 2008; Xing et al., 2005), chemical vapor deposition (CVD) (Amiza et al., 2009), sol–gel deposition (Liu et al., 2006), solvothermal and hydrothermal growth (Srivastava et al., 2012). The two latter are the most convenient because they provide precise control over the size, crystallinity and shape distribution of nanostructures. These properties can be varied by changing experimental parameters such as solvent, temperature, pH, reaction time, type of the precursor and surfactant. Thus, zinc oxide nanostructures with a vast range of morphologies can be synthesized by using appropriate additives in solvent phase and altering the reaction parameters specially the pH.

To the best of our knowledge, there is no study using species having bifunctional activity like those aminoacids, whose isoelectrical pH could be held as precise scaling agents to study the effect of controlled pH over the morphology of final product. In this article, we use a solvothermal process to synthesize various morphologies of zinc oxide under auto-controlled pH conditions occurring by adding amino acids such as lysine, arginine and cysteine to a water-ethanolic solution zinc acetate. An advantage

* Corresponding author. Fax: +98 21 44580762.
E-mail address: Tarlani@ccerci.ac.ir (A. Tarlani).

http://dx.doi.org/10.1016/j.bios.2014.09.063
0956-5663/

of the amino is also their effect on the shape and size of the products. Basic and acidic species such as urea and oxalic acid were used as additives to investigate their effects on the morphologies.

Such prepared nanostructures have been tested as non-enzymatic glucose biosensors. Although glucose is an essential biomolecule of the human life, its excessive amounts in the blood stream can cause serious health problems. Metal oxide compounds have devoted a lot of attentions in the area of glucose sensing (Rahman et al., 2010). Among these type of materials, ZnO nanostructures with unique advantage including appropriate band gap, optical transparency, non-toxicity characteristics, highly chemical stability, ease of fabrication, electrochemical activity and high electron transfer properties which makes them one of the most promising material for glucose biosensing applications (Li et al., 2012). Different zinc oxide nanostructures have been utilized in enzymatic glucose sensors (Kong et al., 2009; Wei et al., 2006; Yang et al., 2009). However, these sensors utilize glucose oxidase enzyme that is expensive and unstable. In this regard, rare efforts started to build non-enzymatic sensors based on zinc oxide by electrochemical methods. Nevertheless, these attempts suffer from using one type of zinc oxide nanostructure, using non-economical gold electrode, applying expensive nafion or undesired detection limit (Baby and Ramaprabhu, 2011; Singh et al., 2012). In this study, various ZnO nanostructures synthesized by new additives and then compared with each other to sense glucose biomolecule through a non-enzymatic approach. The simple and cheap glassy carbon electrode (GCE) modified with multi-walled carbon nanotube (MWCNT) were employed for this analysis. Finally the best nanobiosensor based on new zinc oxide nanostructures with the highest sensitivity will introduce.

Table1
Summary of the experimental conditions and the corresponding morphologies.

Sample	Starting reagents	Treatment	Product[a]	Morphology
1	Zinc acetate, lysine	Autoclave	PZL	Hexagonal-rod
2	PZL	Calcination	ZL	Hexagonal-rod
3	Zinc acetate, lysine, urea	Autoclave	PZLU	Cubic-like
4	PZLU	Calcination	ZLU	Nanoparticle
5	Zinc acetate, lysine, oxalicacid	Autoclave	PZLO	Cubic-like
6	PZLO	Calcination	ZLO	Rock candy-like
7	Zinc acetate, arginin	Autoclave	PZA	Quasi spherical
8	PZA	Calcination	ZA	Quasi spherical
9	Zinc acetate, arginin, urea	Autoclave	PZAU	Nanopowders
10	PZAU	Calcination	ZAU	Nanosheet
11	Zinc acetate, arginin, oxalic acid	Autoclave	PZAO	Cubic-like
12	PZAO	Calcination	ZAO	Nanopowder
13	Zinc acetate, cysteine	Autoclave	PZC	Sphere
14	PZC	Calcination	ZC	Nanopowder
15	Zinc acetate, cysteine, urea	Autoclave	PZCU	Brain-like
16	PZCU	Calcination	ZCU	Groundnut-like
17	Zinc acetate, cysteine, oxalicacid	Autoclave	PZCO	Pussy willow-like
18	PZCO	Calcination	ZCO	Spherical

Reaction conditions: zinc acetate (0.4 mmol); water–ethanol 1:1 v/v (100 mL); amino acid (0.5 mmol); with (or without) urea or oxalic acid (0.7 mmol); autoclaveat 180 °C for 18 h; calcination at 800 °C for 1 h with the ramping rate of 1 °C/min.

Note: All products which calcinated at 800 °C are pure ZnO but we show them with different names to remember their precursors easily.So there is no any difference between for instance, ZCO and ZLU because both of them are pure ZnO.

[a] P stands for precalcination or as-prepared products; Z for zinc; L forlysine; A for argentine; C for cysteine; U for urea and O for oxalate.

2. Materials and methods

2.1. Chemical reagents and apparatus

All used chemical reagents were pro analysis grade purchased from the Merck Chemical Company and used without purification. The powder X-ray diffraction (XRD) patterns were recorded on a Bruker D8 ADVANCE diffractometer using Cu-K_α radiation ($\lambda = 1.5418$ A°). Scanning electron microscopy (SEM) images were obtained with the LEO 1455 apparatus. Infrared spectra were recorded on a FT-IR spectrometer Bruker (IFS-88) in KBr matrix in the range of 400–4000 cm^{-1}. Thermal gravimetric analysis (TGA) carried out on a Netzsch (TGA F209) instrument with the heating rate of 5 °C/min under air, in a flow of 25 ml/min from 25 to 800 °C. Electrochemical analysis carried out using AUTOLAB-state-100 instrument.

2.2. Synthesis of zinc oxide nanostructures

In a typical experimental procedure, 0.4 mmol of zinc acetate, 0.5 mmol of amino acid (lysine, arginin or cysteine) and a 100 mL solution of distilled water–ethanol (1:1 v/v) were mixed with vigorous stirring at room temperature to reach a clear solution (S). This latter was transferred into a stainless steel teflon-lined autoclave and heated at 180 °C for 18 h. Cooling to room temperature leads to white precipitated powders which were isolated by filtration (Samples 1, 7 and 13 in Table 1). Then they were calcinated at 800 °C for 1 h to give samples 2, 8 and 14, respectively.

To test the effect of additives on this new formulation, 0.7 mmol oxalic acid was added to S, which was treated as above to afford Samples 5, 11 and 17 to obtain 6, 12 and 18 respectively. The same process with urea as the additive led to 3, 9 and 15 which provide 4, 10 and 16. The summary of the synthetic conditions is collected in Table 1.

2.3. Preparation of ZnO/MWCNT/GCE sensor and electrochemical characterizations

0.5 g of multi-walled carbon nanotube (MWCNT) in 20 mL nitric acid (14.67 N) was refluxed for 36 h. Then it was thoroughly washed with distilled water to reach the pH = 5. Calcinated ZnO nanostructures (0.24 g) in 10 mL of distilled water and 15 mL of ethylene glycol treated with 0.08 g of carboxylated multi-walled carbon nanotube (MWCNT-COOH) under ultrasonic condition for half an hour. Then it was stirred for 20 h at 80 °C. Finally the suspension centrifuged, washed with distilled water and ethanol. Then it dried in an oven at 60 °C to obtain ZnO/MWCNT. 0.05 g of ZnO/MWCNT dispersed ultrasonically in minimum amount of DMF and then stirred for 24 h. 10 μL of this suspension dropped on glassy carbon electrode (GCE) and dried at 50 °C. Before glucose sensing, the electrode tested in phosphate buffer solution (PBS) with pH = 7 prepared from NaH_2PO_4 and Na_2HPO_4. Also the electrode was tested in 0.01 M of ferri/ferro cyanide ($Fe(CN)_6^{3-/4-}$). Finally the electrode applied as a sensor in desired solution of glucose. Interference study for the best biosensor (ZCO/MWCNT/GCE) carried out with addition of 0.1 mM dopamine (DA), 0.1 mM uric acid (UA), 0.1 mM ascorbic acid (AA) and 0.1 mM fructose at different time intervals. The experiment accomplished in PBS while the working potential was held at 0.12 V (Baby and Ramaprabhu, 2011). The reproducibility test essayed for three different ZCO/MWCNT/GCE biosensors in 10 mM of glucose concentration. To investigate the stability and repeatability of the biosensor, ZCO/MWCNT/GCE was tested twelve times in 10 mM of glucose concentration. This biosensor (which was stored at room temperature) tested again for investigating the stability of the electrode for the same glucose concentration. Also, detecting of

the glucose in the bare simulated body fluid (SBF) as a human blood plasma carried out for negative control purpose (Xu et al., 2009). Positive control was performed by adding 50 μL of certain concentration of glucose into 25 mL of SBF. The mentioned test shows the ability of the sensor for measuring the blood glucose concentration.

3. Results and discussion

Structurally, wurtzite zinc oxide has space group of *C6mc* with lattice parameters of $a=0.3296$ and $c=0.52065$ nm. The structure of ZnO can be portrayed as alternatively stacked planes of tetrahedrally coordinated O^{2-} and Zn^{2+} ions along c axis. Mode of bonding and structural arrangement in the ZnO crystal lattice gives a special polarity to its surfaces, most commonly to that of basal planes. The oppositely charged ions place at different sides of unit cell for wurtzite ZnO, making dipolar surfaces of positively charged Zn (0001) and negatively charged O ($000\bar{1}$) (Wang, 2004). Unless other facets composing the ZnO's crystal structure which also undergo a massive surface reconstruction (Chen et al., 2000; Emanetoglu et al., 1999), ZnO ± (0001) surfaces are flat, stable and without reconstruction (Sunandan and Joydeep, 2009). The other commonly studied facets for ZnO are ($2\bar{1}\bar{1}0$) and ($01\bar{1}0$), which have lower energy surfaces than (0001) facets. Thus, based on these structural facts about ZnO wurtzite, in recent years most of studies have been directed on investigation of parameters that affect the size and morphology of the zincite crystals. Among all, parameters such as temperature, time and reactants have been confirmed as playing crucial roles in the controlled synthesis of the ZnO architectures.

Since natural molecules of special functionality such as amino acids or other bio molecules could lead to a more controlled growth strategy in architecting different ZnO morphologies, the effect of different pH and amino acids was studied in detail.

Throughout our studies, the molar ratio of Zn/amino acid was adjusted at about 1:1.25. To study the effect of acidic or basic conditions on the growing, we used oxalic acid and urea in approximate amounts 1.75:1 to Zn^{2+} ions in the procedure. Indeed, considering recent studies in the related field, these conditions have been believed to be at the forefront of critical values to the final morphologies in wurtzite structures (Wu et al., 2008), aside helping evaluator through realizing the importance of the amino acid′s role in directing and assembling structures (Zhang et al., 2006).

3.1. Morphology and structural analysis of lysine based syntheses

XRD patterns of precalcinated lysine, lysine–urea and lysine–oxalic acid samples are depicted in Fig. 1a, c and e, respectively. Patterns collected for PZL production a first stepare assigned to ZnO phase, while the patterns collected for compounds PZLU and PZLO corresponded to phase mixtures in which the ZnO patterns can be traced as one of the major phases existing in these compounds. However, the calcination of these three samples led to corresponding ZL, ZLU and ZLO products in which all the patterns are the same and all confirm the ZnO crystal structures for aforementioned products (Fig. 1b, d and f). Peaks at angels of $2\theta=31.6°$, 34.2°, 36.0°, 47.4°, 56.5°, 62.7°, 67.7° and 68.9° of these patterns can be assigned to ($10\bar{1}0$), (0002), ($10\bar{1}1$), ($10\bar{1}2$), ($11\bar{2}0$), ($10\bar{1}3$), ($11\bar{2}2$) and ($20\bar{2}1$) diffraction planes respectively, and are characteristics of the hexagonal wurtzite ZnO phase with JCPDS card file numbers of 05-0664 and 36-1451. Indeed, the patterns exhibit sharp and narrow peaks which confirm the high crystallinity of these samples. Corresponding SEM images of PZL, ZL, PZLU, ZLU, PZLO and ZLO are shown in Fig. 1. PZL and ZL (Fig. 1a and b), display rod-shaped nanostructures with the hexagonal cross section. It can also be seen that, by using lysine lonely, there is no notable difference in the morphology of products before and after calcinations even though their XRD patterns are slightly different in peak intensities. The average length of ZnO nanorods is about 2 μm with a cross section size in the range 400–650 nm. SEM images of the products of lysine with urea (as an additive) are also shown in this figure. However, results show that before calcination, almost undesirable cubic-like PZLU morphology was formed in which size distribution were ranged at 1000–1700 nm (Fig. 1c). However, after the calcination, morphology was majorly changed and nanoparticles in the range 50–90 nm with uniform

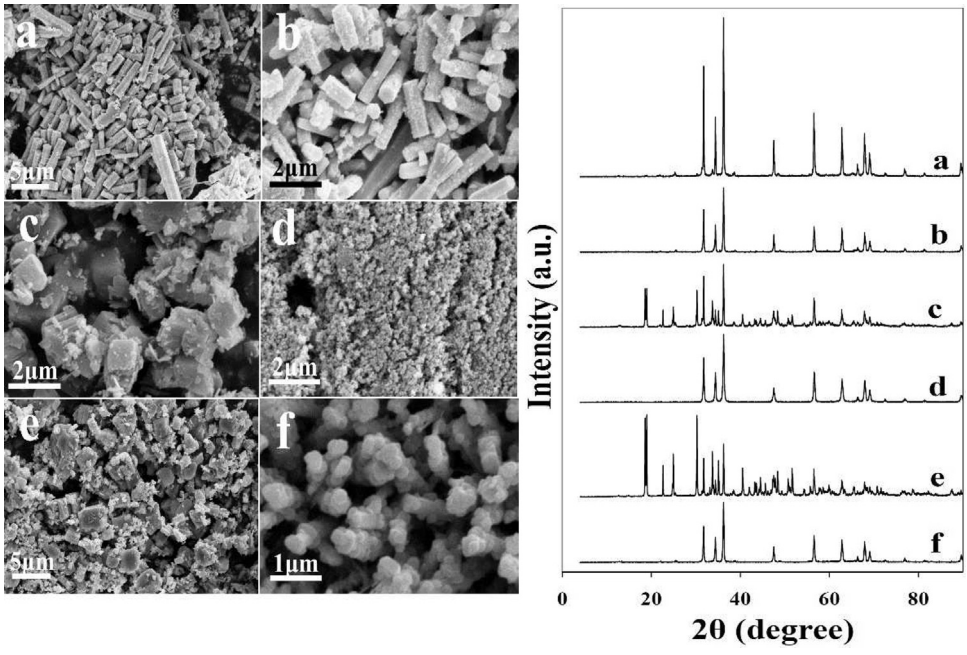

Fig. 1. XRD patterns and SEM images of the lysine based products with (or without) urea or oxalic acid before and after calcination: (a) PZL, (b) ZL, (c) PZLU, (d) ZLU, (e) PZLO and (f) ZLO.

Please cite this article as: Tarlani, A., et al., Biosensors and Bioelectronics (2014), http://dx.doi.org/10.1016/j.bios.2014.09.063

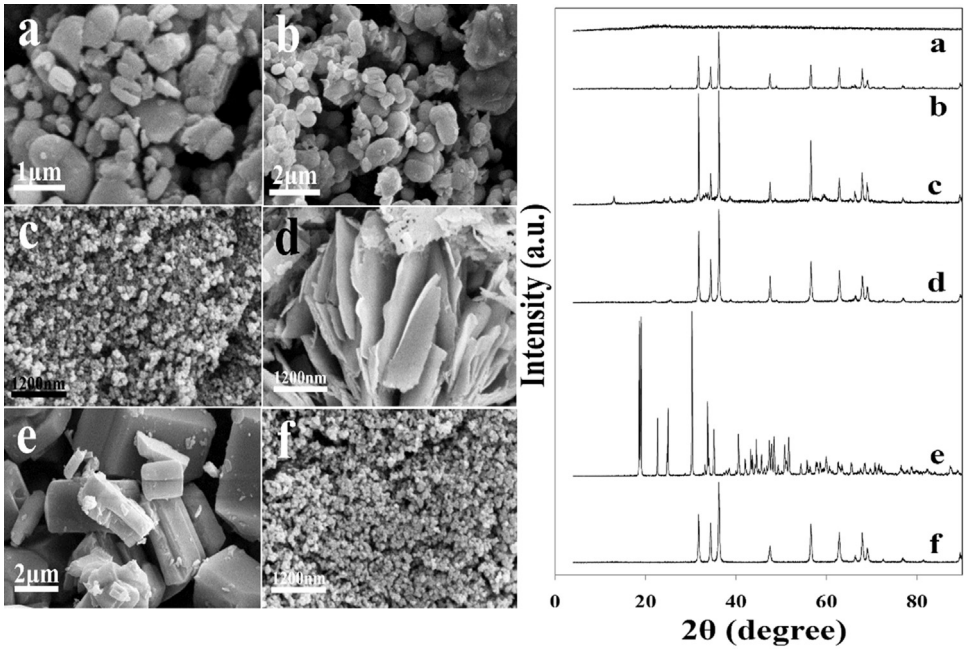

Fig. 2. XRD patterns and SEM images of the arginine based products with (or without) urea or oxalic acid before and after the calcination: (a) PZA, (b) ZA, (c) PZAU, (d) ZAU, (e) PZAO and (f) ZAO.

distribution were obtained (Fig. 1d). The same process was also repeated for the lysine–oxalic acid system. As being depicted in Fig.1e, before the calcinations, a cubic-like phase with inappropriate morphology formed; however, after the calcination it seems that this morphology was converted to uniform rock candy-like structures ranging at 200–450 nm (Fig. 1e and f).

3.2. Morphology and structural analysis of arginine based syntheses

Figs. 2a to f correspond to SEM images of PZA, ZA, PZAU, ZAU, PZAO and ZAO. PZA and ZA (before and after calcination) were synthesized from zinc acetate and arginine as the only directing agent. The captured morphology for PZA shows three dimensional quasi spherical nanostructures (Fig. 2a). The morphology of ZA is more uniform than that of PZA, in which the size range of the particles are fallen at about 400–800 nm (Fig. 2b). PZAU, which is formed with urea and arginine, is isolated as nano powders in the size range 50–90 nm with uniform distribution (Fig. 2c). By calcinations, these nanoparticles were almost converted into nanosheets with 30 to 60 nm thicknesses and 1.5 to 2.5 μm length (Fig. 2d). In the case of the oxalic acid as the second additive, (Fig. 2e,f), PZAO exhibits cubic-like structures with 1.5 to 4μm height and about 1 μm length. Calcinations led to nanopowders with uniform distribution in the range 60-90 nm. XRD pattern of

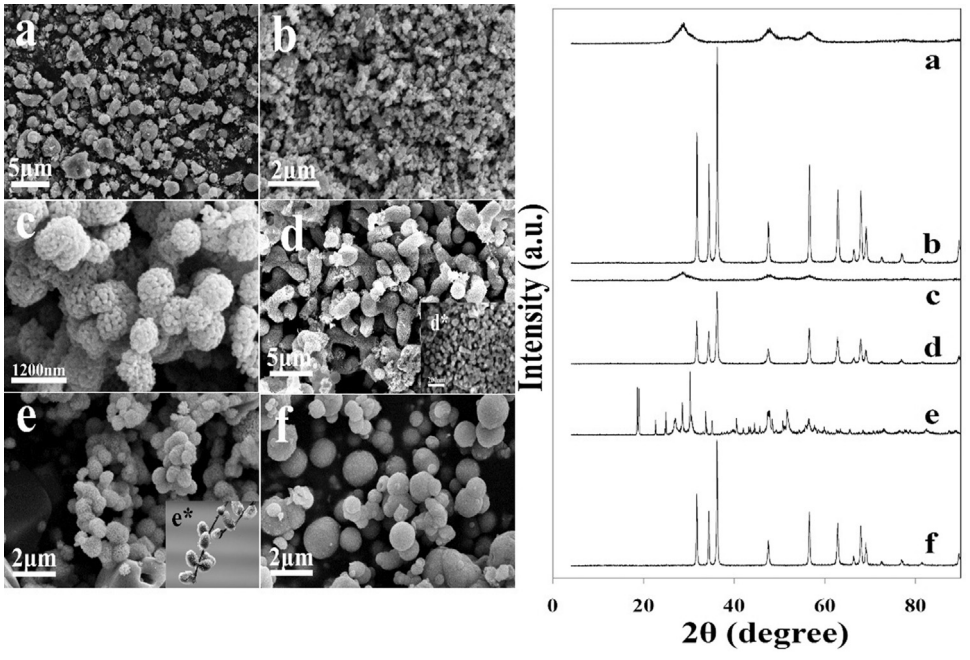

Fig. 3. XRD patterns and SEM images of the cysteine based products with (or without) urea or oxalic acid before and after the calcination: (a) PZC, (b) ZC, (c) PZCU, (d) ZCU, (e) PZCO, (f) ZCO; d*, ZCU in 200 nm magnification; e*, PZCO is resembling a real image of pussy willow.

Please cite this article as: Tarlani, A., et al., Biosensors and Bioelectronics (2014), http://dx.doi.org/10.1016/j.bios.2014.09.063

the as-made zinc acetate-arginine (PZA) showed an amorphous phase while the calcination product of ZA exhibited the ZnO phase (Fig. 2a and b). By adding urea and oxalic acid and after the calcination, the same pure wurtzite phase observed. By adding urea to zinc acetate-arginine and after autoclave treatment, PZAU was formed. XRD pattern of this sample was mostly assigned to pure zinc oxide (Fig. 2c). By substitution of oxalic acid with urea, PZAO was formed. XRD pattern of this sample verified two major phase of zinc oxalate (Ni et al., 2011) and zinc oxide (Fig. 2e).

3.3. Morphology and structural analysis of cysteine based syntheses

PZC, ZC, PZCU, ZCU, PZCO and ZCO correspond to the cysteine, cysteine–urea and cysteine–oxalic acid and corresponding calcinated samples. Surprisingly, both XRD patterns of PZC and PZCU showed ZnS crystalline phase, while, pattern of PZCO exhibited zinc oxalate phase (Fig. 3a, c and e). Wurtzite crystalline phases were however obtained by calcination of these three samples (Fig. 3b, d and f). As shown in the SEM images, before calcination of the sample PZC, spherical nanostructures with the size about 1200 nm were obtained. Whereas, after the calcination morphology of the corresponding product changed and the nanopowders in the range 70–150 nm were obtained (Figs. 3a and b). In the cysteine–urea formulation brain-like structures with the size in the range 500–1200 nm were seen for the as-made PZCU sample (Fig. 3c).After the calcinations, the morphology transformed to novel groundnut-like nanostructures with the sponge-like surface (Fig. 3d). They are not nanosize but it seems that these structures are accumulation of nanosized spheres in which sizes are in the range 25–50 nm (Fig. 3d). By adding oxalic acid to cysteine, PZCO and ZCO samples were obtained. Before calcinations novel pussy willow-like structures in the range 150–300 nm were resulted (Fig. 3e). Their lint sizes are in the range 10–30 nm. Surprisingly, after the calcination, the morphology converted to nanospheres with 500 to 1500 nm in diameter (Fig. 3f).

Full description of FT-IR and TG analyzes of the samples could be found in supplementary information (Figs. S1 and S2).

3.4. Repeatability, reproducibility, stability and interference study of the biosensor

Fig. 4 shows CV of simple GCE in PBS, ZnO/MWCNT/GCE in PBS and ZnO/MWCNT/GCE in 10 mM glucose for the nine calcined ZnO morphologies. The total time for the sample detection was about 60 s. Spherical ZCO, ZLU nanoparticles, and ZAU nanosheet exhibited the best response to 10 mM of glucose solution with sensitivity of 64.29, 63.48 and 42.85 μA/cm^2 mM respectively which is comparable with another report (Zang et al., 2007). The reproducibility test carried out for three different ZCO/MWCNT/GCE electrodes in 10 mM of glucose concentration with standard deviation (RSD) of 3.862. In order to

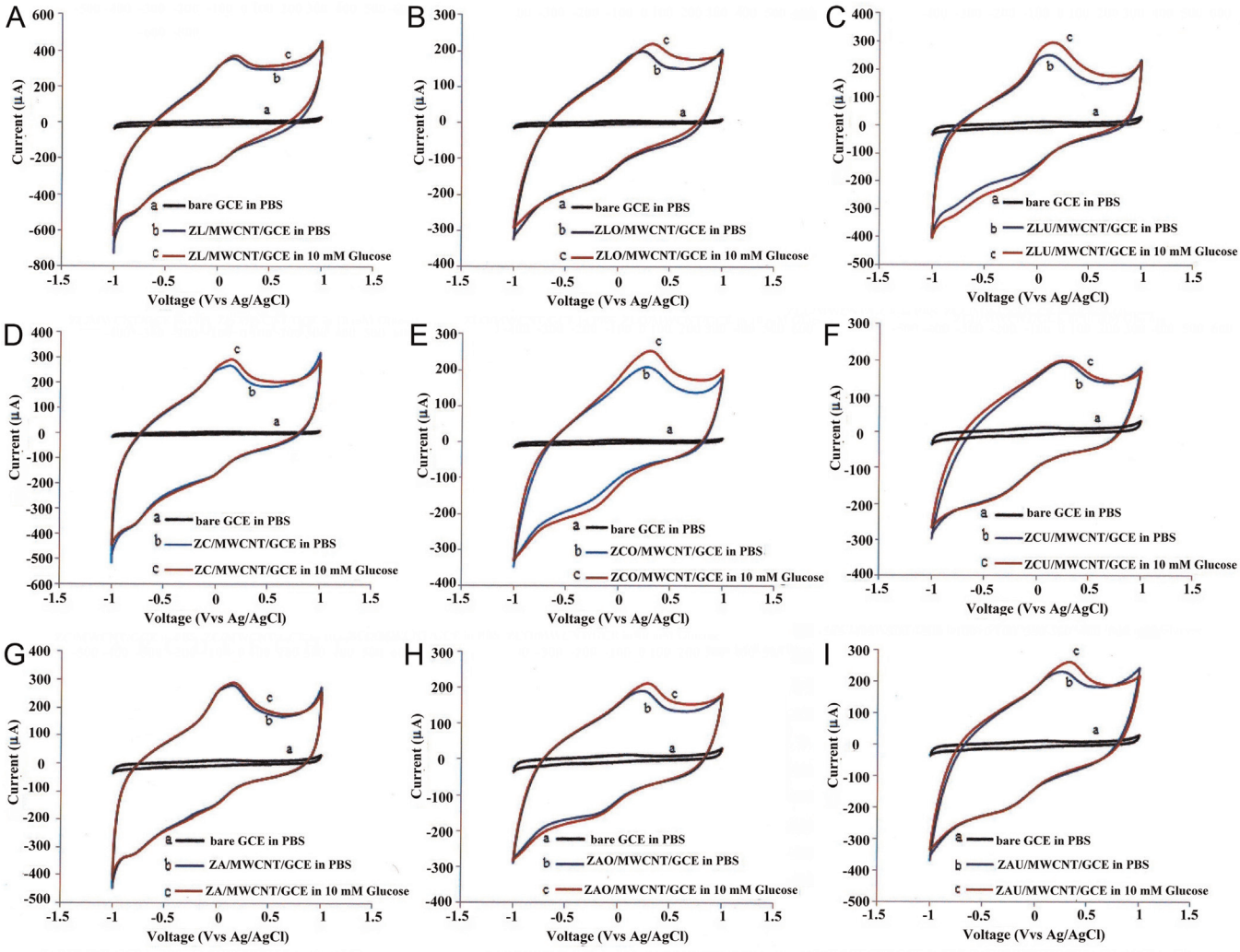

Fig. 4. CV of simple CE in PBS, ZnO/MWCNT/GCE in PBS and ZnO/MWCNT/GCE in 10 mM glucose for the samples: (A) ZL, (B) ZLO, (C) ZLU, (D) ZC, (E) ZCO, (F) ZCU, (G) ZA, (H) ZAO and (I) ZAU.

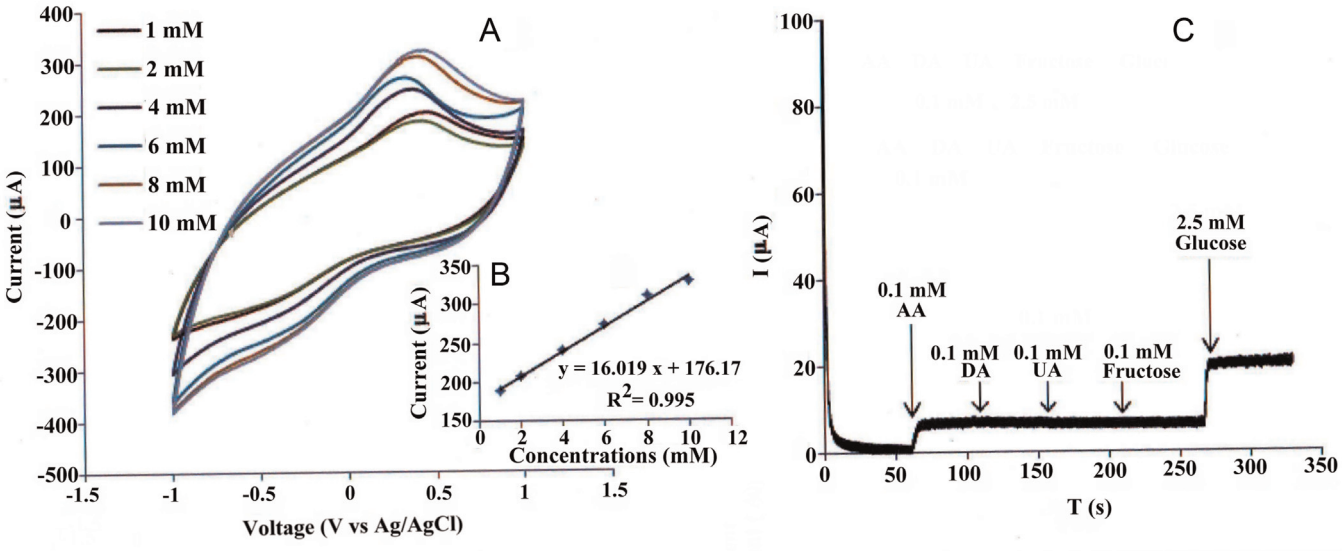

Fig. 5. ZCO/MWCNT/GCE applied in (A) plotting CV of changing glucose concentration from 1 to 10 mM in PBS, (B) Calibration curve of this biosensor (C) Interference test at +0.12 V with 2.5 mM glucose and other electroactive species including 0.1 mM AA, 0.1 mM DA, 0.1 mM UA and 0.1 mM fructose in PBS.

essay the repeatability of the biosensor, ZCO/MWCNT/GCE was repetitively applied for measuring 10 mM of glucose concentration for twelve times. The measured RSD was 0.396. The mentioned biosensor which was stored at room temperature (since a month ago) was tested again to investigate the stability of the electrode. No significant reduction in the performance of the biosensor was observed during the sensing of 10 mM of the glucose. These results exhibited that the biosensor has acceptable stability, repeatability and reproducibility.

To verify the sensitivity of ZCO/MWCNT/GCE biosensor as a function of glucose concentrations, 1, 2, 4, 6, 8 and 10 mM of glucose solution prepared for biosensing at room temperature (Fig. 5A). Calibration curve of the biosensor with the correlation coefficient of 0.995 is depicted in this figure (Fig. 5B). The detection limit of the biosensor was 0.82 mM (3 SD/m). As can be seen, enhancement of the current response observed while the concentration of glucose was increased. Triplicates at each concentration could be found in Fig. S3. Also, electrochemical response of the interfering dopamine (DA), uric acid (UA), ascorbic acid (AA) and fructose at the concentration of 0.1 mM, was examined for ZCO/MWCNT/GCE biosensor at working potential of +0.12 V in PBS (Fig. 5C). Results revealed that DA, UA and fructose do not show the response in the presence of 2.5 mM of glucose. Also, the amount of glucose is detectable in the presence of 0.1 mM of AA (Liu et al., 2013).

3.5. Real sample analysis

Moreover, ZCO/MWCNT/GCE electrode was utilized as a biosensor to detect glucose in blood plasma. For this purpose, a simulated body fluid (SBF) was selected for determining the glucose level (Kiani et al., 2014; Xu et al., 2009). Firstly, sensing the bare SBF solution showed a null response during the experiment (negative control). The same experiment carried out by adding a standard solution of glucose to SBF. Subsequently, the electrochemical response increased clearly. The result exhibited that the biosensor showed a dose dependence response (Fig. S4). Also, it confirmed that, biosensing of the glucose by means of ZCO/MWCNT/GCE electrode is feasible without any interference.

This is an advantage for this electrode that without using nafion or glucose oxidase, glucose is detectable in the presence of electroactive species (Baby and Ramaprabhu, 2011). Therefore, it could be concluded that, simple and low cost ZCO/MWCNT/GCE biosensor can sense the glucose efficiently and selectively.

4. Conclusions

Crystalline nanostructures of ZnO have been synthesized by solvothermal process through the reaction of zinc acetate with amino acids (lysine, arginine and cystein) and, eventually, oxalic acid or urea. These nanostructures have been supported on glassy carbon electrodes, and these latter have been used to determine the glucose concentration of aqueous solutions. The best sensitivity was obtained using the nano sensor of ZCO/MWCNT/GCE with the sensitivity of 64.29 μA/cm^2 mM. Also this electrode tested in different concentration of glucose from 1 to 10 mM with acceptable sensitivity response. Interference study on DA, UA, AA and fructose (0.1 mM) applied for the simple ZCO/MWCNT/GCE biosensor at working potential of +0.12 V in PBS. Results showed that the sensor can detect glucose readily. Finally, the biosensor revealed a good dose dependence response for glucose in the presence of SBF.

Acknowledgment

The authors would like to appreciate financial support of this research Project (No: 90004099) by Iran National Science Foundation (INSF). Authors would like to thank Mr. Amirreza Ariamoghadam, Dr. Sayahi and Dr. Kiani for their helps as well as Chemistry & Chemical Engineering Research Center of Iran.

Appendix A. Supplementary material

Supplementary data associated with this article can be found in the online version at http://dx.doi.org/10.1016/j.bios.2014.09.063.

References

Akhavan, O., 2010. ACS Nano 4 (7), 4174–4180.
Amiza, S., Mamat, M.H., Khusaimi, Z., Sahdan, M.Z., Abdullah, S., Rusop, M., Hartini, A.R., 2009. Mater. Res. Innov. 13 (3), 207–210.

Baby, T.T., Ramaprabhu, S., 2011. J. Nanosci. Nanotechnol. 11 (6), 4684–4691.
Botello-Méndez, A.R., López-Urías, F., Terrones, M., Terrones, H., 2008. Nano Lett. 8 (6), 1562–1565.
Briseno, A.L., Holcombe, T.W., Boukai, A.I., Garnett, E.C., Shelton, S.W., Fréchet, J.J.M., Yang, P., 2010. Nano Lett. 10 (1), 334–340.
Chen, Y., Bagnall, D., Yao, T., 2000. Mater. Sci. Eng.: B 75 (2–3), 190–198.
Cui, Y., Wei, Q., Park, H., Lieber, C.M., 2001. Science 293 (5533), 1289–1292.
Dai, Z.R., Pan, Z.W., Wang, Z.L., 2003. Adv. Funct. Mater. 13 (1), 9–24.
De La Rica, R., Matsui, H., 2008. Angew. Chem.-Int. Ed. 47 (29), 5415–5417.
Deng, G., Ding, A., Cheng, W., Zheng, X., Qiu, P., 2005. Solid State Commun. 134 (4), 283–286.
Emanetoglu, N.W., Gorla, C., Liu, Y., Liang, S., Lu, Y., 1999. Mater. Sci. Semicond. Process. 2 (3), 247–252.
Gao, P.X., Wang, Z.L., 2004. Appl. Phys. Lett. 84 (15), 2883–2885.
Ju, S., Facchetti, A., Xuan, Y., Liu, J., Ishikawa, F., Ye, P., Zhou, C., Marks, T.J., Janes, D.B., 2007. Nat. Nanotechnol. 2 (6), 378–384.
Kiani, M.A., Tehrani, M.A., Sayahi, H., 2014. Anal. Chim. Acta 839 (0), 26–33.
Kim, H.S., Myung, Y., Cho, Y.J., Jang, D.M., Jung, C.S., Park, J., Ahn, J.P., 2010. Nano Lett. 10 (5), 1682–1691.
Kong, T., Chen, Y., Ye, Y., Zhang, K., Wang, Z., Wang, X., 2009. Sens. Actuators B: Chem. 138 (1), 344–350.
Kong, X.Y., Ding, Y., Yang, R., Wang, Z.L., 2004. Science 303 (5662), 1348–1351.
Kong, X.Y., Wang, Z.L., 2003. Nano Lett. 3 (12), 1625–1631.
Kumar, B., Lee, K.Y., Park, H.K., Chae, S.J., Lee, Y.H., Kim, S.W., 2011. ACS Nano 5 (5), 4197–4204.
Lao, J.Y., Huang, J.Y., Wang, D.Z., Ren, Z.F., 2003. Nano Lett. 3 (2), 235–238.
Lee, Y.J., Ruby, D.S., Peters, D.W., McKenzie, B.B., Hsu, J.W.P., 2008. Nano Lett. 8 (5), 1501–1505.
Li, J., Ma, S., Liu, X., Zhou, Z., Sun, C.Q., 2012. Chem. Rev. 112 (5), 2833–2852.
Liu, B., Zeng, H.C., 2003. J. Am. Chem. Soc. 125 (15), 4430–4431.
Liu, S., Yu, B., Zhang, T., 2013. Electrochim. Acta 102 (0), 104–107.
Liu, X., Wang, J., Zhang, J., Yang, S., 2006. Mater. Sci. Eng. A 430 (1-2), 248–253.
Liu, Y., Tong, Y., 2008. J. Nanosci. Nanotechnol. 8 (3), 1101–1109.
Lu, J.G., Ye, Z.Z., Huang, J.Y., Zhu, L.P., Zhao, B.H., Wang, Z.L., Fujita, S., 2006. Appl. Phys. Lett. 88 (6), 063110–063113.
Morales, A.M., Lieber, C.M., 1998. Science 279 (5348), 208–211.
Nam, Y.S., Magyar, A.P., Lee, D., Kim, J.W., Yun, D.S., Park, H., Pollom Jr, T.S., Weitz, D. A., Belcher, A.M., 2010. Nat. Nanotechnol. 5 (5), 340–344.
Ng, H.T., Li, J., Smith, M.K., Nguyen, P., Cassell, A., Han, J., Meyyappan, M., 2003. Science 300 (5623), 1249.
Ni, L., Wang, L., Shao, B., Wang, Y., Zhang, W., Jiang, Y., 2011. J. Mat. Sci. Technol 27 (6), 563–569.
Pan, H., Feng, Y.P., 2008. ACS Nano 2 (11), 2410–2414.
Pan, Z.W., Dai, S., Rouleau, C.M., Lowndes, D.H., 2004. Angew. Chem.-Int. Ed., 44; , pp. 274–278.
Rahman, M.M., Ahammad, A.J.S., Jin, J.-H., Ahn, S.J., Lee, J.-J., 2010. Sensors 10 (5), 4855–4886.
Shen, X., Allen, P.B., Muckerman, J.T., Davenport, J.W., Zheng, J.C., 2007. Nano Lett. 7 (8), 2267–2271.
Shi, J., Grutzik, S., Wang, X., 2009. ACS Nano 3 (6), 1594–1602.
Singh, K., Umar, A., Kumar, A., Chaudhary, G.R., Singh, S., Mehta, S.K., 2012. Sci. Adv. Mater. 4 (9), 994–1000.
Srivastava, V., Babu, E.S., Han, S.K., Lee, H.S., Lim, D.S., Kim, H., Kim, D., Hong, S.K., 2012. J. Nanosci. Nanotechnol. 12 (2), 1328–1331.
Sunandan, B., Joydeep, D., 2009. Sci. Technol. Adv. Mater. 10 (1), 013001.
Tandra, G., Subhajit, B., Soumitra, K., Apurba, D., Supriya, C., Subhadra, C., 2008. Nanotechnology 19 (6), 065606.
Wang, X., Song, J., Li, P., Ryou, J.H., Dupuis, R.D., Summers, C.J., Wang, Z.L., 2005. J. Am. Chem. Soc. 127 (21), 7920–7923.
Wang, Z.L., 2004. J. Phys. Condens. Matter 16 (25), R829–R858.
Wang, Z.L., 2007. Appl. Phys. A: Mater. Sci. Process 88 (1), 7–15.
Wang, Z.L., 2008. ACS Nano 2 (10), 1987–1992.
Wei, A., Sun, X.W., Wang, J.X., Lei, Y., Cai, X.P., Li, C.M., Dong, Z.L., Huang, W., 2006. Appl. Phys. Lett. 89 (12).
Wu, Q., Chen, X., Zhang, P., Han, Y., Yan, Y., Li, S., 2008. Cryst. Growth Des. 8 (8), 3010–3018.
Xing, Y.J., Xi, Z.H., Zhang, X.D., Song, J.H., Wang, R.M., Xu, J., Xue, Z.Q., Yu, D.P., 2005. Appl. Phys. A: Mater. Sci. Process 80 (7), 1527–1530.
Xu, W., Gao, Q., Xu, Y., Wu, D., Sun, Y., Shen, W., Deng, F., 2009. Powder Technol. 191 (1–2), 13–20.
Yang, K., She, G.-W., Wang, H., Ou, X.-M., Zhang, X.-H., Lee, C.-S., Lee, S.-T., 2009. J. Phys. Chem. C 113 (47), 20169–20172.
Zang, J., Li, C.M., Cui, X., Wang, J., Sun, X., Dong, H., Sun, C.Q., 2007. Electroanalysis 19 (9), 1008–1014.
Zhang, B., Ye, X., Hou, W., Zhao, Y., Xie, Y., 2006. J. Phys. Chem. B 110 (18), 8978–8985.

Please cite this article as: Tarlani, A., et al., Biosensors and Bioelectronics (2014), http://dx.doi.org/10.1016/j.bios.2014.09.063